Inkjet Printed Silver Electrodes on Macroporous Paper for a Paper-Based Isoelectric Focusing Device

Cristina Gaspar[1], Tiina Sikanen[2], Sami Franssila[1] and Ville Jokinen[1a]

[1] Department of Materials Science and Engineering, School of Chemical Technology, Aalto University, Aalto FI-00076, Finland. Email: ville.p.jokinen@aalto.fi

[2] Division of Pharmaceutical Chemistry and Technology, Faculty of Pharmacy, FI-00014 University of Helsinki, Helsinki, Finland

Inkjet Printed Silver Electrodes on Macroporous Paper for a Paper-Based Isoelectric Focusing Device

Cristina Gaspar[1], Tiina Sikanen[2], Sami Franssila[1] and Ville Jokinen[1a]

[1] Department of Materials Science and Engineering, School of Chemical Technology, Aalto University, Aalto FI-00076, Finland. Email: ville.p.jokinen@aalto.fi

[2] Division of Pharmaceutical Chemistry and Technology, Faculty of Pharmacy, FI-00014 University of Helsinki, Helsinki, Finland

We demonstrate a combined printing process utilizing inkjet printing of silver electrodes and solid-ink technology for printing hydrophobic wax barriers for fabricating paper microfluidic devices with integrated electrodes. Optimized printing parameters are given for achieving conducting silver lines on top of macroporous chromatography paper down to 250 µm - 300 µm resolution. Electrical characterization and wicking experiments demonstrate that the printed silver patterns are simultaneously conductive and porous enough to allow reliable capillary wicking across the electrodes. The combined wax and silver printing method is used for fabrication of paper microfluidic isoelectric focusing devices for separation and concentration of proteins.

a) Author to whom correspondence should be addressed. Electronic mail: ville.p.jokinen@aalto.fi

Introduction

Printed intelligence can provide electronic, chemical and biological functionalities to rigid and flexible substrates. Microfluidics and lab-on-a-chips are currently being developed with a promise of devices with higher sensitivity, lower sample volumes, smaller scale, disposability and low cost [1,2]. Recently, there has been a trend toward paper based microfluidics for clinical diagnostics[3,4]. Paper microfluidic devices can be mass produced and are thus very cheap and disposable. Furthermore paper offers natural wicking, good contrast for colorimetric assays and is environmentally friendly[3,5,6].

Printing techniques are widely used to fabricate a variety of paper microfluidic devices[4]. Microfluidic paper-based analytical devices (μPADs) have gained increasing attention since the introduction of low-cost wax-printing for fabrication of complex microfluidic networks on hydrophilic chromatography paper[7]. Inkjet technology can be used to pattern reagents on paper for analysis[8–10] and to deposit conductive patterns [6,11,12]. Under optimal conditions, inkjet printing can achieve a resolution below 50 μm. Such a high resolution can be achieved by tuning the ink viscosity, nozzle size and the surface properties. Inkjet printing is compatible with mass-manufacturing and roll-to-roll production, to reach high throughput, high speed and low cost printing of commercial microfluidic devices[8]. Wax-printing (i.e., solid-ink technology) has been commonly used as a printing method for fabricating hydrophobic barriers for microfluidic paper-based devices[13,14]. It is a simple fabrication method but the resolution is inherently limited to hundreds of micrometers due to wax melting step required to fill the pores to form the barriers[10]. Screen-printing has been used as a fabrication method for both microfluidics channels[15–17] and integrated electrodes[18]. Typically, screen-printing requires highly viscous inks, in the range of 1000 – 10000 cP, or higher, and, therefore, resolution of the printed structures is low. However, screen-printing allows 2D or 3D printed structures and is generally fast and low-cost. Flexo-printing is a versatile printing method, which uses less viscous inks and allows for higher printing resolution of microfluidics channels[19]. All these printing methods are generally compatible with large-scale fabrication methods, due to the small number of process steps they require and compatibility with industrial equipment.

Paper microfluidics utilizes the hydrophilic nature of cellulose and the porous nature of paper for achieving wicking of liquids. The wicking process depends on the pore size and connectivity of the paper[20]. However, porous substrates are very challenging for printing electronics due to their roughness and wettability. On porous substrates, the resolution is expected to be significantly worse and sufficient conductivity is more difficult to achieve. Surface tailoring can be utilized to smoothen the surface[21] but this adds the complexity and the coatings will also affect the wicking and adsorption properties of the paper. Recently, Whitesides et al. [22] listed the five major limitations of current paper-based electrochemical systems. The common theme among the limitations is that the electrodes are commonly either printed only on the surface of the paper, which limits the effective area and prevents stacked designs, or alternatively the printed electrodes block the pores which either prevents or significantly slows down the wicking.

Here, we demonstrate an optimized fabrication process for implementation of inkjet-printed electrodes on macroporous paper. The electrodes are further integrated with a paper microfluidic isoelectric focusing (IEF) device created by wax printing on the same highly porous and unmodified chromatography paper as the conductive silver patterns. The parameters of the printing processes are optimized to achieve two competing goals: reliable capillary wicking, which benefits from large open pores, and conducting lines with low resistance, which requires percolating networks of metal. We utilize the obtained devices for protein separation by IEF, which is an established technique for proteomic analyses and facilitates separation of amphoteric compounds based on their isoelectric point (*pI*). The porous chromatography papers readily mimic the horizontal, hydrophilic and porous gels typically used in IEF. However, apart from isotachophoretic sample preconcentration[23,24], IEF or other modes of electrokinetic separation have hardly been performed on paper microfluidic devices before.

Materials and methods

Paper substrates and wicking experiment

Whatman no. 1 chromatography paper (VWR International Oy, Helsinki, Finland) was used as the paper substrate for all printing purposes. The paper is cellulose-based, with weight of 87 g/m^2, thickness of 180 µm and an average pore size of 11 µm.

For the wicking experiment, the printed papers were suspended horizontally on air so that there was no gravity gradient or contact between the paper and any substrate. Deionized water was introduced from one end of the substrate and the time it takes for the liquid front to reach various predetermined locations was recorded. The reported values are averages and standard deviations (SD) of three measurements.

Silver printing

A commercially available silver (Ag) nanoparticle colloidal ink, from Advanced Nano Products Co., Ltd. was used in this work. The metallic nanoparticle ink contains around 30 w% Ag nanoparticles in a polar solvent, with a particle diameter of 5-10 nm. Inkjet-printing was carried out using a piezoelectric multi nozzle, from Dimatix (DMP-2831), 10 pL cartridges, with 16 nozzles. The drop spacing was optimized and set to 20 µm. While printing, the substrate temperature was set to 60 °C, to improve the evaporation of the solvent from the ejected droplets. Infra-red (IR) oven (Infrared IC heater T-962, Puhui Electric Technology Co., Ltd) was used for sintering the ink with 800 W output power. After the printing of the structures, the substrates were introduced in an IR-oven at 150 ^{0}C, for 7 minutes. UV-sintering was also tested, with a CAMAG, 12 V oven. The samples were put inside the oven, with five lamps of 8 W power and 254 nm wavelength, for 60 minutes. The silver patterns were visually inspected by scanning electron microscopy (SEM) (TM-1000, Hitachi, Japan), to assess the quality of the printed structures, both the top surface and cross-sections and baksides. For the cross section SEMs, the paper was cut by scissors. The linewidths were measured with the Dimatix printer camera and built-in software, (n=3, average and SD reported). The conductivity of the printed lines was measured with a Digital multimeter BST BS1704 (n=10, average and SD reported).

Wax printing

The fluid barriers were defined by printing hydrophobic wax on the back side of the chromatography paper using Xerox Phaser 8560DN solid ink color printer (Varimport

Oy, Turku, Finland) following the method adopted from Carrilho et al.[13]. The solid ink is a mixture of hydrocarbons and hydrophobic carbamates with melting point of about 120°C. After printing, the wax was melted on a Stuart Scientific SH3D digital hot plate (Stafford, UK) at +150°C for 3 min. During melting, the chromatography paper was sandwiched between two aluminum foils to protect the paper from adsorbed contaminants. An external, planar weight (1-2 kg) was placed on top of the foil to ensure uniform heat transfer from the hot plate to the paper and penetration of the melted wax into the pores of the chromatography paper. The printed width of the wax barriers was 1 mm, which was enough to ensure penetration of the wax through the pores to the front side of the paper in 3 min. After melting, the width of the barriers was approximately 2 mm.

Isoelectric focusing

Cytochrome *c* from bovine heart, myoglobin from equine heart, and ampholyte (pH 3-10) used for isoelectric focusing were purchased from Sigma Aldrich (Steinheim, Germany). Hydrochloric acid and sodium hydroxide were from Riedel-de Haën (Seelze, Germany). Water was purified with a Milli-Q water purification system (Millipore, Molsheim, France). The IEF setup is shown in Figure 1. Before IEF experiments, the sample was diluted in 2% ampholyte (pH 3-10) solution and about 7 µL of this solution was applied to the hydrophilic area between the silver electrodes. The printed silver patterns slowed down the capillary flow across the electrodes and thus the areas outside of electrodes could be subsequently filled with the anolyte (1.2 mol/L hydrochloric acid) and the catholyte (2.0 mol/L sodium hydroxide) solutions by dispensing them (V~50 µL) to the absorbent pads at respective ends (Fig. 1b). As soon as the hydrophilic areas were filled with the anolyte and the catholyte, high voltage was applied *via* alligator clips between the anode (+) and the cathode (-) electrodes. The IEF current was monitored over an amperometer coupled in series with the IEF device.

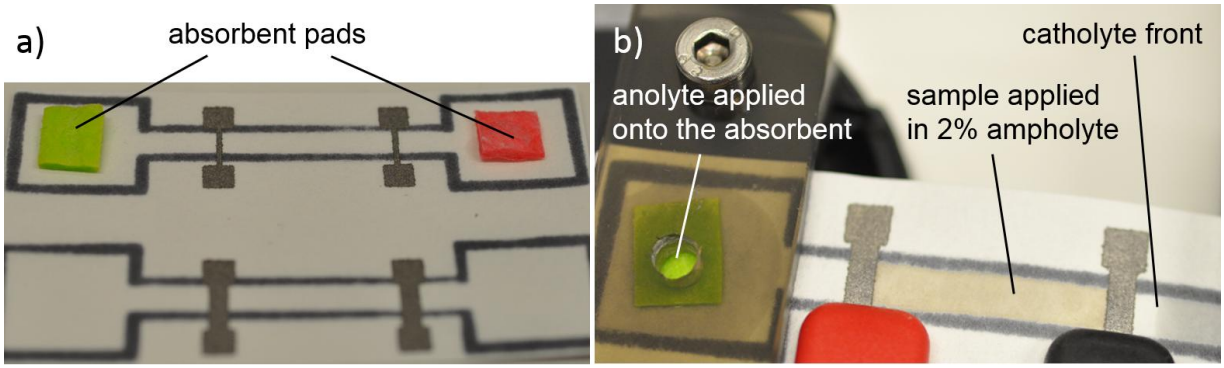

Figure 1. Paper isoelectric focusing with integrated electrodes. (A) Two wax patterns (after melting) with silver electrodes and absorbent pads (green pad=anolyte, red pad=catholyte). (B) Illustration of the filling step before the IEF experiments. The red and black alligator clips attached to the silver electrodes represent the anode (+) and cathode (-) poles, respectively.

Results and Discussion

Silver printing parameters for porous substrates

The paper substrates were used without any pre-treatment prior to silver printing. As the paper is highly porous, the normal inkjet-printing parameters, recommended by the ink manufacturer, lead to rapid penetration of the ink into paper which did not translate into conducting lines. Instead a custom printing procedure was developed. The substrate temperature was set to 60 ºC to promote the ink solvent evaporation and solidify the ink faster, so that wicking would be reduced and percolation increased. The second parameter to be optimized was the droplet spacing and we concluded that 20 µm was the optimal value. This allowed sufficient layer coverage, due to a droplet overlapping on the substrate surface. Although a large quantity of ink was dispensed, it was necessary to fill all the voids of the porous substrate to ensure the conductivity of the inkjet-printed patterns after sintering. The third optimized parameter was to use the lowest possible jetting frequency (1 kHz) allowed by the Dimatix printer in order to avoid/reduce the interference of the mechanical movements from the stage movement, affecting the final printing resolution and its quality. The firing voltage was tuned individually and set to 23 ± 1 V for each nozzle.

Combined process for wax and silver printing

The geometries of the IEF devices incorporating printed silver electrodes and hydrophobic wax are shown in Figure 2. Two nominal linewidths were tested for the silver electrodes, 0.5 mm and 3 mm. The length between the contact pads was 10 mm and the distance between the electrodes (in IEF) was 20 or 22 mm depending on the line width. The number of printed layers is a tradeoff: single layers are faster to print and to sinter and leave more pores open for wicking. On the other hand, printing multiple layers results in better conductivity. We tested printing 1, 2, and 3 layers and compared their performance in terms of wicking and electrical conductivity.

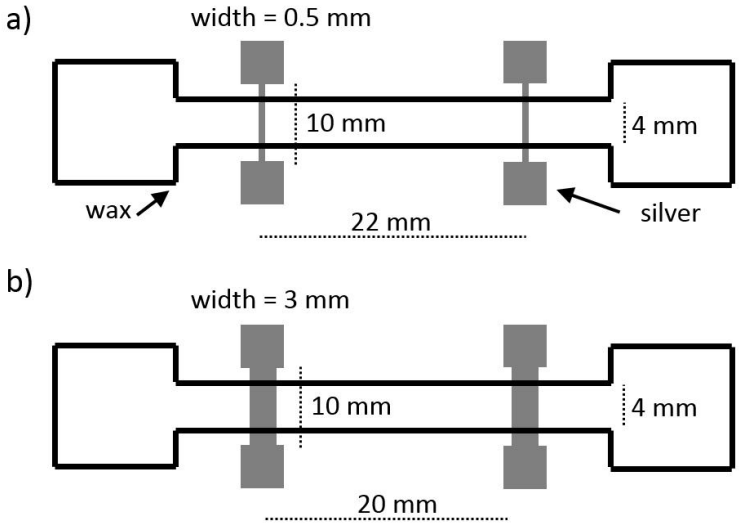

Figure 2. Inkjet printed paper IEF devices. a) Device with 0.5 mm nominal width of the electrode. b) Device with 3 mm nominal width of the electrode.

Two approaches were pursued for combined wax and silver printing: either wax-first or silver-first. The approaches were compared in terms of printing quality, conductivity of the printed lines and the fabrication complexity. The main difference between the two approaches is the thermal load for wax melting and silver particle sintering. In both

cases the aligning of the two layers was done based on standard paper sizes and the inherent accuracy of the printers themselves, which was sufficient for this study.

In the wax-first approach, no substrate heating was used during the silver printing in order to avoid reflow of the wax. Otherwise the parameters were as explained in the previous section. Without the use of substrate heating, the ink penetration onto the porous substrate was high. Because of this, the conductivity of the lines and the resolution of the patterns was compromised. As IR-sintering was not possible due to wax melting, UV sintering was the only possibility with this approach. The printed patterns were sintered efficiently with UV, due to the localized energy focusing on the metal lines, without affecting the wax pattern. Ten millimeters long conductive lines printed by a single layer had resistances of 224 ± 1 kΩ for the 3-mm-wide and 177 ± 14 kΩ for the 0.5-mm-wide lines.

In the silver first approach, substrate temperature of 60 ºC could be used and there were no limitations for sintering conditions due to wax melting. Furthermore, the wax melting (3 min at 150ºC, after sintering) did not in any way adversely affect the printed silver electrodes. This approach proved to be clearly simpler and more versatile from the fabrication point of view and resulted in better resolution of the patterns. The resistances of 3 mm and 0.5 mm wide lines (single layer) were 690 ± 230 Ω and 1200 ± 500 Ω respectively, which are between 2 and 3 orders of magnitude lower than the corresponding lines with the wax first approach. Also, there was no problem utilizing IR sintering (as well as UV sintering) in the silver first approach. Because of this, all further results reported were done using the silver first approach and IR-sintering.

Printing resolution

Achieving good printing resolution on top of a macroporous substrate with high wicking capability is a challenge. The strategy was to print several layers, in order to uniformly coat the pores and to use heated substrate during silver printing to promote evaporation

of the ink solvent and thus prevent excessive spreading. Table 1 presents the nominal and measured linewidths of conducting silver lines for 1, 2 and 3 printed layers.

Table 1. Linewidths as a function of number of printed layers (Data presented as mean ± SD, n = *3).*

Nominal width (µm)	**Real width (µm) 1 layer**	**Real width (µm) 2 layers**	**Real width (µm) 3 layers**
3000	2529 ± 12	2381 ± 6	2468 ± 40
500	851 ± 49	741 ± 44	740 ± 43

On smooth substrates (e.g. polymer sheets), a higher number of printed layers will result in wider features due to spreading of the added ink toward the edges of the printed patterns. In this work, the linewidths were largely unaffected by the number of printed layers (Table 1) thanks to the fact that the ink partially filled the macropores instead of spreading. The linewidths for the 3 mm lines were approximately 0.5 mm under the target, independent of the number of printed layers, while the linewidths for the 0.5 mm lines were approximately 0.3 mm over the target with the chosen parameters.

With just one printed layer, the coverage of the ink is somewhat uneven, whereas with two and three printed layers, a more continuous line is obtained (Figure 3, top-view images). The cross-section SEM images show that after the third printed layer, the ink has penetrated to the entire depth of the paper, while the porosity is still maintained. This is also confirmed by SEM images taken from the backside of the samples. The silver ink was clearly visible from the backside on the sample with 3 printed layers but not on the samples with 1 and 2 layers. The optimized drop spacing during the inkjet-printing method allowed us to reduce the number of printed layers while increasing the quality of the printed pattern

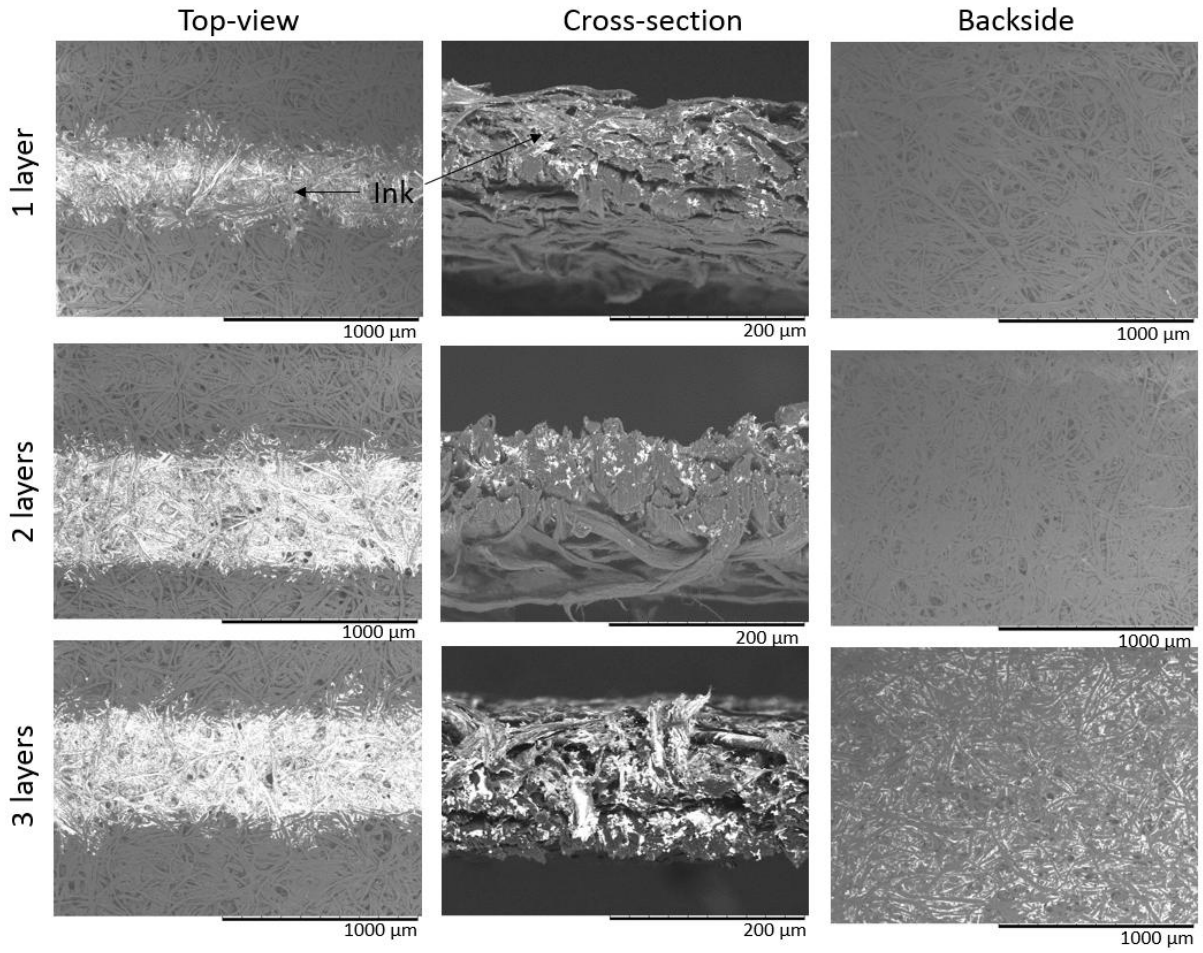

Figure 3. SEM micrographs of inkjet-printed Ag lines on chromatography paper. The top-view SEMS:s are of 500 micron lines, while the cross sectional and the backside images are from 3000 micron lines.

To further develop the printing resolution we also developed a second, high resolution, printing process. The fabrication process and electrical characterization is explained in the Electronic Supplementary Information.

Figure 4 presents the results utilizing the high resolution printing process. Fig. 4a-b shows a test pattern consisting of closely a packed array of silver pads. With this process, the narrowest conducting lines were 236 µm ± 32 µm (Fig. 4c) wide and the narrowest gaps required for no cross conductivity were 330 µm ± 61 µm and 285 µm ± 31 µm in the horizontal and vertical printing direction respectively (Fig 4d). Narrower

lines and gaps than these could be printed but they did not reliably have proper conductivity or lack of cross conductivity, respectively.

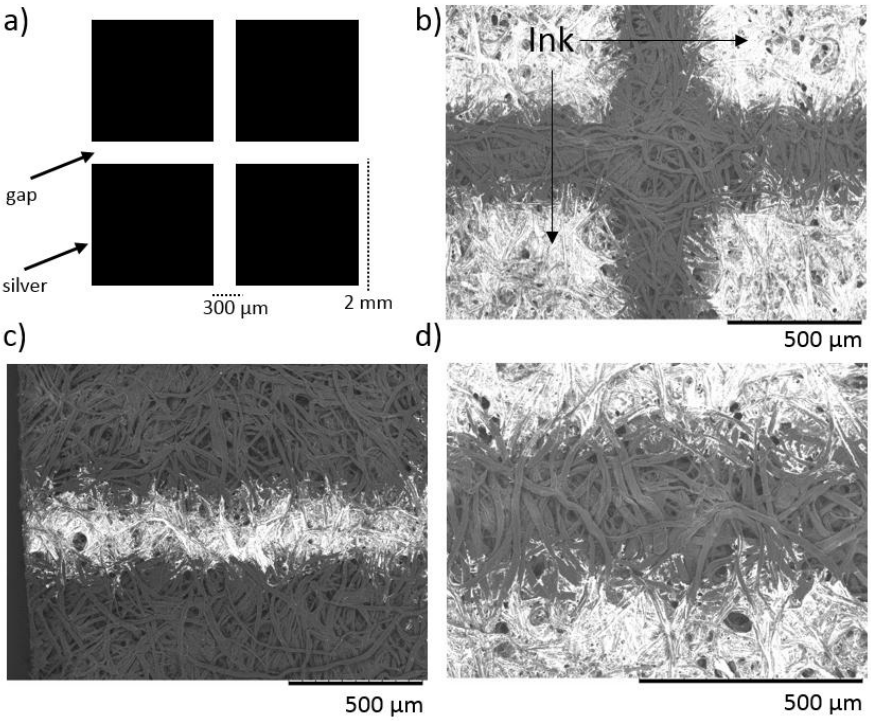

Figure 4. High resolution patterns (3 printed layers). a) schematic of an array of four electrode pads in close proximity. b) SEM of the electrode pad array. c) The narrowest reliably obtained gap. d) The narrowest reliably obtained line.

The limit to the minimum gap resolution is clear from the SEM images (Fig. 4d): the individual fibers and pores are in a random orientation with respect to the printed pattern, which leads to stochastic spreading of the ink by around 100 µm or more from the edge of the designed pattern. If a particular fiber configuration spans the gap between two conducting lines, a silver bridge can form between them.

The limit to the minimum printed linewidth is not as clear. It was possible to print narrower lines, but they were not guaranteed to be conductive (although many of them were). A possible reason is that the thinner the line is, the more probable it is that a fiber/pore configuration that prevents the ink spreading (by a geometrical valving effect) spans the entire width of the line, which would lead to a lack of percolation.

Conductivity

Resistance measurements were performed on the inkjet-printed silver lines to assess the dependency of the resistance on the number of printed layers. The lines had the same dimensions as the IEF device, 10 mm length and either 3 mm or 0.5 mm nominal width. The resistances are shown in Table 2.

Table 2. Resistance as a function of number of printed layers (Data presented as mean ± SD, n = *10).*

Nominal width (µm)	**1 layer Resistance (Ω)**	**2 layers Resistance (Ω)**	**3 layers Resistance (Ω)**
3000	690 ± 230	10 ± 2	4 ± 1
500	1200 ± 500	35 ± 7	16 ± 4

With just one printed layer, the resistances were in the kilo-ohm range. With two layers, the conductivity was improved by approximately 1-2 orders of magnitude compared to the single layer and resistance obtained with three layers was roughly half of the resistance obtained with two layers.

Wicking

Figure 5 shows the results of wicking experiments that were performed in order to confirm that the chromatography paper supported capillary wicking despite the printed silver patterns. This was crucial in terms of the performance of the paper microfluidic IEF device in order to assure liquid contact between the anolyte/catholyte and the sample solution . The tests were performed with samples that had a total of four alternating 3 mm and 0.5 mm wide silver lines, 1 cm apart, as indicated in Figure 5. The results show that water was able to reliably wick across the silver electrodes although the printed patterns did slightly slow down the wicking rate. The observed slowdown is likely due to decreased pore size and (possibly) altered contact angle. The wicking rates followed closely the Washburn[25] relation. The wicking rates were calculated by best fit into $x^2 = kt$, where x is the distance, t is the time and k is the wicking rate, and they were 5.71 mm^2/s for the unmodified blank paper, 5.04 mm^2/s for a single printed silver layer and 4.63 mm^2/s for 3 printed silver layers. Since the differences in the wicking rates

were modest, three printed layers were used on the IEF device in order to ensure proper electrical contact.

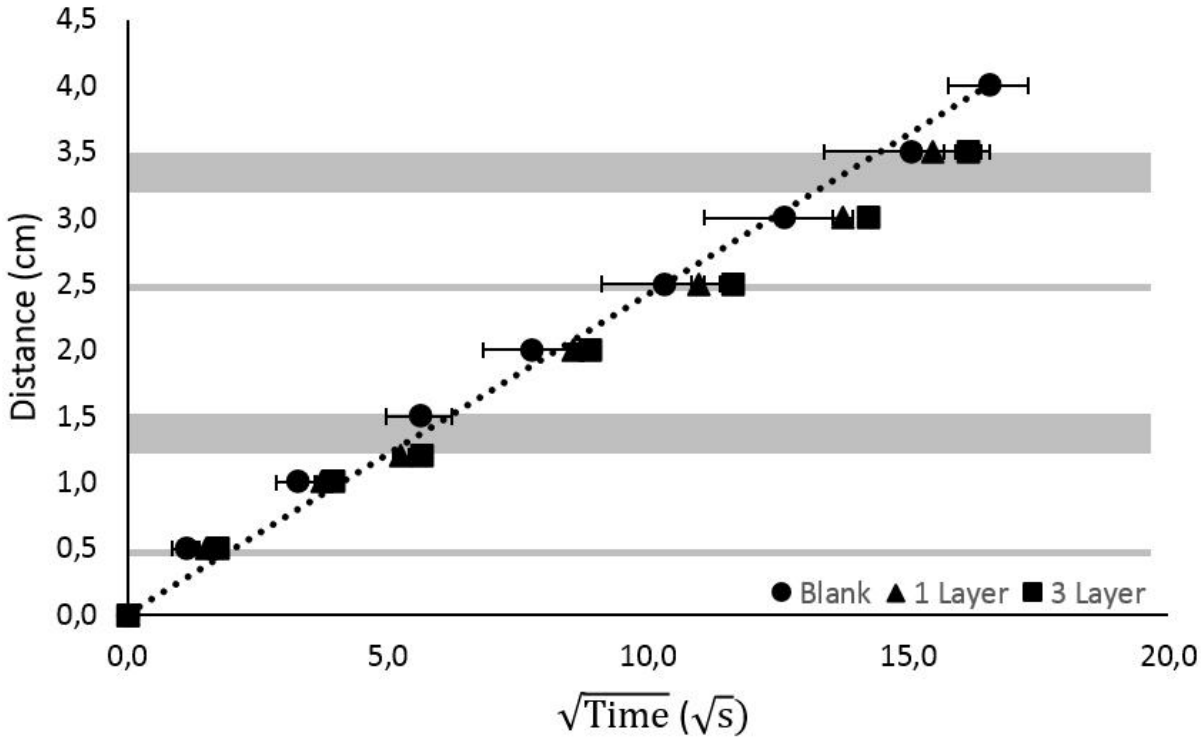

Figure 5. Effect of printed silver lines on the wicking behavior. The locations of the inkjet-printed electrodes are marked with gray. The dashed line shows the best fit to the blank sample. (Data presented as mean ± SD, n = *3).*

Isoelectric focusing of proteins

Most paper-based assays reported so far are targeting clinical applications where sensitivity is not an issue, e.g., blood glucose detection with typical in vivo concentrations in the mmol/L level)[26] . At the same time, many diagnostic needs cannot be met due to the limited sensitivity of the mPADs in detecting, e.g., protein biomarkers. In a prior study, Rosenfeld and Bercovici[23] introduced paper-based isotachnophoresis (ITP) for increasing the sensitivity of mPADs. Up to 1000-fold sample enrichment was achieved for a fluorescent dye (DyLight 650). However, ITP is primarily a sample enrichment technique with limited resolving power due to overlapping analyte zones. To improve its separation capacity, ITP needs to be coupled to another (electrokinetic)

separation technique, such as zone electrophoresis (i.e., transient ITP), which increases the complexity of the mPAD.

In this study, we developed a mPAD for IEF, which is another electrokinetic separation technique and particularly well-established for simultaneous separation and enrichment of amphoteric compounds, such as proteins and peptides. In IEF, a pH gradient is created with help of carrier ampholytes and proteins separate according to their isoelectric point (*p*I) at the respective position of the pH gradient. Increasing the focusing time results in sharper sample bands until the sample components reach zero charge.

A visible enrichment and separation of the model proteins, cytochrome *c* (pI 9.6; M_r 11.7 kDa) and myoglobin (pI 6.8-7.4, M_r 17.8 kDa) was obtained by paper-based IEF in 5-10 min (Figure 6). Such long operation time is challenging for any open-to-air paper microfluidic device due to evaporation. Here, the absorbent pads used at the cathode and anode of the IEF channel, helped eliminate the evaporation effect and keep the system wet over the required period of time. To avoid excessive Joule heating, the focusing voltage was increased step-wise, in 200V increments, from U=200V and until U=1000V (100-500 V/cm) as the electrical current decreased indicating formation of the pH gradient. Any significant leaching of the Ag ink or degradation of the electrodes was not observed during IEF.

On our IEF device, the distance between the silver electrodes defined the effective separation length (L_{eff}) and, together with the channel width, the sample volume. Here, the applied sample volume was 7 mL (corresponding to 35 mg protein), but the total volume can be easily increased or decreased on demand by simply adjusting the width of the wax defined IEF channel and the distance between the ink-jet printed electrodes. Thus, toward clinical diagnostics (i.e., identification of protein biomarkers at low level), the detection sensitivity can be further improved by increasing the total protein amount (greater sample volume) and the focusing efficiency (longer IEF run time and/or adjusted ampholyte composition) without much affecting the final position of the focused target protein with respect to anode and cathode. As proteins and peptides are the most common classes of diagnostic biomarkers, there is a wide range of customized,

recombinant antibodies available (for targeted identification) that can be dispensed at predefined locations of the IEF channel (based on expected, known pI of the target protein). Thus, by combining paper-based IEF, as demonstrated in this work, with ink-jet printed antibody arrays, it is possible to push the detection sensitivity of the current mPADs toward clinically relevant concentrations.

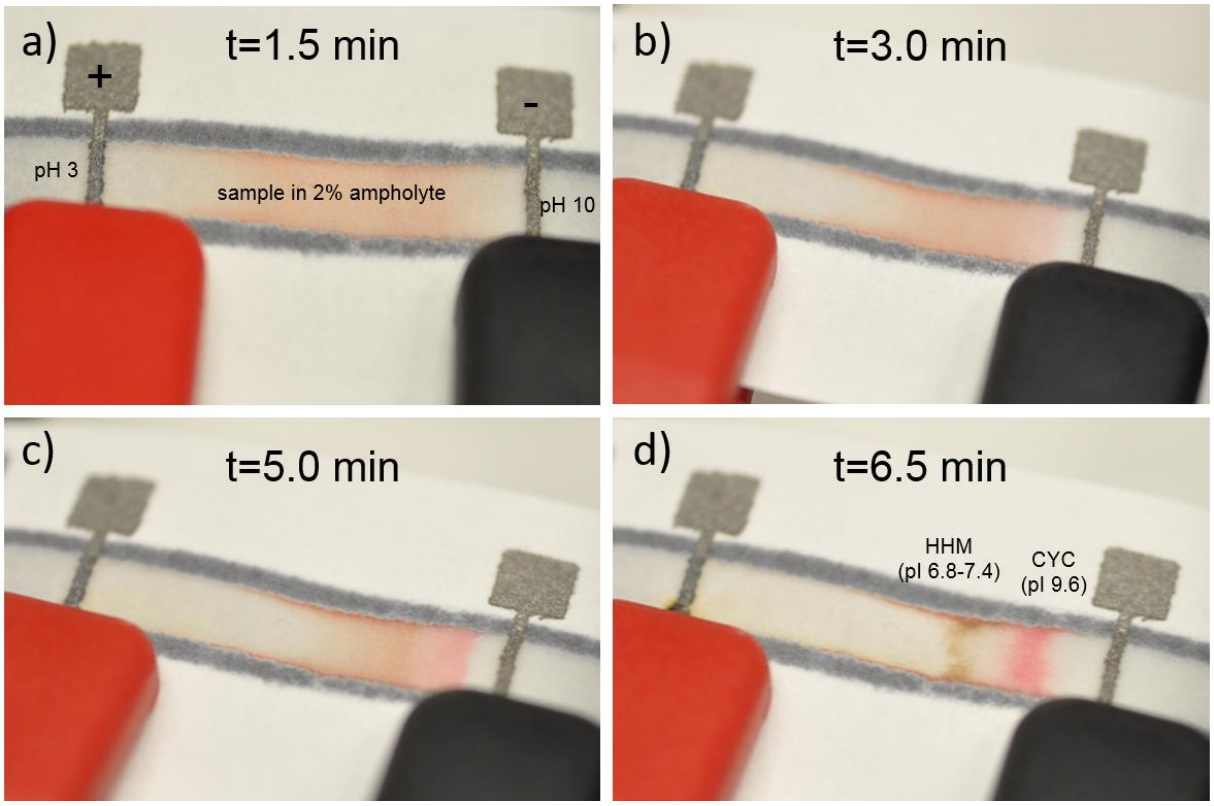

Figure 6. Illustration of the IEF separation of cytochrome c (pI 9.6, red in color) and myoglobin (pI 6.8-7.4, brown in color), both 5 µg/µL in 2% ampholyte (pH 3-10), on a porous chromatography paper along with time. The separation voltage was applied between the anode (+, red clip) and the cathode (-, black clip) in increments of 200V every 60 s. The photographs were taken at (A) t=1.5 min, Usep=400V, (B) t=3.0 min, Usep=600V, (C) t=5.0 min, Usep=1000V, after which the voltage was increased to Usep=1500V to fully resolve the proteins in t=6.5 min (D).

Discussion

The wicking and the conductivity results and the SEM micrographs together show that after three printing cycles, the silver ink penetrates to the entire depth of the paper while maintaining the porosity of the chromatography paper for capillary wicking. Because of this, the electrodes can overcome many of the known limitations of paper-based electrochemical systems[22]. The surface area of the electrodes is high, since the electrodes printed by our process penetrate deeply or fully into the paper. Also, pores of the paper remain open and large enough for capillary wicking through the electrodes with only moderate slowdown of the wicking rate. Finally, the full penetration achieved by 3 printed layer allows interlayer electrical connections to be made for more complex devices.

Conclusion

We have shown that by carefully optimizing the printing parameters, it is possible to fabricate an all-printed paper microfluidic device with wax barriers and integrated inkjet-printed silver electrodes. The macroporous chromatography paper is a challenging substrate for creating a percolating network necessary for good conductivity, but this can be overcome by printing three layers on top of each other. The maximum resolution for conductive lines was 250 µm for linewidth and 300 µm for the gap between adjacent lines. The lowest resistances of 10 mm long and 0.5 mm or 3 mm wide lines were in the 1 Ω -10 Ω range. The integrated electrodes were utilized for protein separation by paper-based IEF which could allow development of µPADs for detecting also lower concentration analytes. In addition, integrated electrodes are feasible for electrochemical detection methods to complement the colorimetric assays commonly used in paper microfluidics.

Supplementary material

See supplementary material for the printing parameters and the electrical characterization of the high resolution silver printing process.

Acknowledgements

Funding from the Academy of Finland (#266820, #297360, #264743) is acknowledged. The research leading to these results has also received funding from the European Research Council under the European Union's Seventh Framework Program (FP/2007-2013) / ERC Grant Agreement n. 311705 (CUMTAS).

[1] A. Arora, G. Simone, G.B. Salieb-Beugelaar, J.T. Kim, and A. Manz, Analytical Chemistry **82**, 4830 (2010).
[2] G. Du, Q. Fang, and J.M.J. den Toonder, Analytica Chimica Acta **903**, 36 (2016).
[3] Y. Xia, J. Si, and Z. Li, Biosensors and Bioelectronics **77**, 774 (2016).
[4] X. Li, D.R. Ballerini, and W. Shen, Biomicrofluidics **6**, 11301 (2012).
[5] A.K. Yetisen, M.S. Akram, and C.R. Lowe, Lab on a Chip **13**, 2210 (2013).
[6] G. Jenkins, Y. Wang, Y.L. Xie, Q. Wu, W. Huang, L. Wang, and X. Yang, Microfluidics and Nanofluidics **19**, 251 (2015).
[7] A.W. Martinez, S.T. Phillips, G.M. Whitesides, and E. Carrilho, Analytical Chemistry **82**, 3 (2010).
[8] B. Feyssa, C. Liedert, L. Kivimaki, L.-S. Johansson, H. Jantunen, and L. Hakalahti, PLoS ONE **8**, e68918 (2013).
[9] K. Abe, K. Suzuki, and D. Citterio, Analytical Chemistry **80**, 6928 (2008).
[10] K. Maejima, S. Tomikawa, K. Suzuki, and D. Citterio, RSC Advances **3**, 9258 (2013).
[11] A. Määttänen, P. Ihalainen, P. Pulkkinen, S. Wang, H. Tenhu, and J. Peltonen, ACS Applied Materials & Interfaces **4**, 955 (2012).
[12] R. Fobel, A.E. Kirby, A.H.C. Ng, R.R. Farnood, and A.R. Wheeler, Advanced Materials **26**, 2838 (2014).
[13] E. Carrilho, A.W. Martinez, and G.M. Whitesides, Analytical Chemistry **81**, 7091 (2009).
[14] B. Kalish and H. Tsutsui, Lab Chip **14**, 4354 (2014).
[15] W. Dungchai, O. Chailapakul, and C.S. Henry, The Analyst **136**, 77 (2011).
[16] H. Zhu, X. Lin, Y. Su, H. Dong, and J. Wu, Biosensors and Bioelectronics **63**, 371 (2015).
[17] Y. Sameenoi, P.N. Nongkai, S. Nouanthavong, C.S. Henry, and D. Nacapricha, The Analyst **139**, 6580 (2014).
[18] W.-J. Lan, E.J. Maxwell, C. Parolo, D.K. Bwambok, A.B. Subramaniam, and G.M. Whitesides, Lab on a Chip **13**, 4103 (2013).
[19] J. Olkkonen, K. Lehtinen, and T. Erho, Analytical Chemistry **82**, 10246 (2010).
[20] R. Masoodi and K.M. Pillai, AIChE Journal NA (2010).
[21] D. Tobjörk and R. Österbacka, Advanced Materials **23**, 1935 (2011).
[22] M.M. Hamedi, A. Ainla, F. Güder, D.C. Christodouleas, M.T. Fernández-Abedul, and G.M. Whitesides, Advanced Materials **28**, 5054 (2016).
[23] T. Rosenfeld and M. Bercovici, Lab Chip **14**, 4465 (2014).
[24] B.Y. Moghadam, K.T. Connelly, and J.D. Posner, Analytical Chemistry **86**, 5829 (2014).
[25] E.W. Washburn, Physical Review **17**, 273 (1921).

[26] J. Noiphung, T. Songjaroen, W. Dungchai, C.S. Henry, O. Chailapakul, and W. Laiwattanapaisal, Analytica Chimica Acta **788**, 39 (2013).